ARTICLE

Check for updates

Time gated Fourier transform spectroscopy as a technique for disentangling short- and long-lived luminescence

Mikkel Baldtzer Liisberg [1✉] & Tom Vosch [1✉]

Overlapping short- and long-lived luminescence signals are often encountered and are not trivial to disentangle in a single measurement. Here, we demonstrate for a broad range of emitters that time gated Fourier transform spectroscopy can be used as a technique to simultaneously capture and temporally disentangle overlapping spectral features of luminescence signals. This allows us to concurrently measure the fluorescence and phosphorescence bands of an organic fluorophore, retrieve the emission of a quantum dot that is overshadowed by an autofluorescent serum solution, and for removing residual laser scatter and ambient room light in an optical filter free configuration. Time gated Fourier transform spectroscopy only requires the introduction of a common-path interferometer to the emission path of a standard time-correlated single photon counting setup; it can function as a technique to both discriminate signals as well as characterize properties of new materials.

[1] Nanoscience Center and Department of Chemistry, University of Copenhagen, Copenhagen, Denmark. ✉email: mbl@chem.ku.dk; tom@chem.ku.dk

Luminescence is ubiquitously used in various fields due to its inherent sensitivity that can be leveraged to provide both qualitative and quantitative information. The sensitivity partially originates from the fact that the signal can be separated either spectrally[1] or temporally[2] from an unwanted background. Other methods for selectively extracting a signal of interest use polarization[3] or frequency modulation[4,5] aspects. Before new luminescent materials are used in applications, characterization of their spectral and temporal response is required in order to determine the best strategy for maximizing the signal to background ratio. Luminescence can also serve as a readout of the electronic structure of newly developed materials[6,7]. Hence, tools for characterizing materials both spectrally and temporally are in demand not only as experimental readout devices but also to investigate the fundamental properties of materials.

A classic spectroscopic device that can measure both spectral and time-resolved information simultaneously is a streak camera where one dimension of the camera chip acts as the energy resolved axis by using, for instance, a diffracting element, and the other axis acts as the temporal axis by deflecting the photons/electrons in time[8,9]. Streak cameras are, however, usually expensive[10], and a more common configuration for recording similar 2D temporal-spectral maps is based on point detectors where the two dimensions are resolved sequentially rather than simultaneously. Experimentally, this is commonly realized with a monochromator in front of a point detector connected to a time-correlated single photon counting (TCSPC) card, where the spectrally resolved decays are constructed in a stepwise manner[11,12]. Another approach is to replace the monochromator with a birefringent common-path interferometer for providing the spectral dimension; this has brought the advantages of Fourier transform (FT) spectroscopy to the visible spectral region[13]. In this approach, a luminescence decay is recorded at every position of the interferometer as it is being scanned over a predefined range. The resulting interferograms are then Fourier transformed, which yields a 2D temporal-spectral map[14].

Here, we demonstrate how the 2D temporal-spectral maps, generated by the introduction of a common-path interferometer to a standard TCSPC setup with a point detector, can be especially useful for characterizing and discriminating luminescence signals that occur on widely different timescales. By time gating numerically in a post-acquisition manner, we are able to create time gated emission spectra, which can disentangle, for example, spectrally overlapping nanosecond lived fluorescence from microsecond lived phosphorescence. Hence, we refer to this technique as time gated Fourier transform spectroscopy (TG-FTS), which combines the optical methodology developed by Perri et al.[15] with the time gating analysis methodology developed by Liisberg et al[16] for a single useful technique. We present a number of cases to demonstrate the numerous material characterization and selective signal recovery applications this method can be used for.

Results and discussion

Principle of TG-FTS. TG-FTS relies on two essential elements, an interferometer and a TCSPC board, which provide spectral and temporal information, respectively; the basics of both will briefly be elaborated upon.

We use a common-path birefringent interferometer (Translating-Wedge-based Identical pulses eNcoding System; TWINS), which allows for collecting spectra in the visible and near-infrared regions with ease[13]. In the TWINS interferometer, emission light is firstly passed through a polarizer (P1 in Fig. 1a) with its transmission axis oriented at 45° with respect to the horizontal axis. Next, it passes through a birefringent block (A), creating two orthogonally polarized beams with a fixed relative delay. The relative delay between the two beams can be tuned from a

negative to a positive value by passing through a second birefringent block (B, with its optical axis orthogonal to A). This block is comprised of a couple of birefringent wedges with a variable effective thickness determined by the insertion of one of the wedges by a length, x. Finally, a second polarizer (P2) projects the two components to a common polarization to impose interference at the detector[13]. Fourier transforming the recorded interferogram yields an emission spectrum after a series of calibrations (see Supplementary Note 1)[14].

In TCSPC, each detected photon gets assigned an arrival time, known as the 'micro-time', which is the time between a detection event and the next synchronization pulse. Collecting all the detected photons into a histogram yields a decay curve on the nanosecond timescale (Fig. 1b). If long-lived luminescence (micro- to milliseconds) is also present, it will appear as an increased background, as the time-to-amplitude converter (TAC) window will usually be too short for the luminescence to decay appreciably. Accordingly, it is possible to gate the collected photons numerically (post-acquisition) based on whether they are in or out of the fluorescence decay window (Fig. 1b; see Supplementary Fig. 3 for gating procedure) and separate the photons based on whether they originate from a short- or long-lived state[16].

For demonstrating TG-FTS, we use a microscope-based setup where we introduced the TWINS interferometer in the emission path and record the micro-time of emitted photons with a TCSPC board (Fig. 1a, see Methods section for a detailed description of the setup). To illustrate the working principle of TG-FTS, we will here consider the hypothetical case of a dual-emissive species with a spectrally overlapping short- and long-lived component. With the setup, a two-dimensional ungated intensity map, $I_{UG}(t, x)$, is produced by recording a decay at every wedge position of the TWINS (Fig. 1c); we will subsequently refer to this as a time-resolved interferometric map (TRIM). Performing a FT along the position axis and applying a series of calibrations (see Supplementary Note 1), leads to a 2D temporal-spectral map, $I_{UG}(t, \lambda)$, that reveals two spectrally overlapping components, which are, however, temporally distinct (Fig. 1c); this is referred to as a time-resolved emission map (TREM). Since the two contributions are distinct in time, it possible to time gate $I_{UG}(t, x)$ numerically, and prepare two new TRIMs (Fig. 1d, e), one which only contains short-lived fluorescence, $I_{Fl,TG}(t, x)$, and another which only consist of long-lived luminescence, $I_{Lu,TG}(t, x)$. It is necessary to correct both $I_{Fl,TG}(t, x)$ and $I_{Lu,TG}(t, x)$ since some luminescence will be present in the time gating window. This is rather straightforward because the luminescence response can be considered as a flat background over the entire TAC window. Fourier transforming these time gated TRIMs (TG-TRIMs), yields time gated TREMs (TG-TREMs) that disentangled the short-lived fluorescence, $I_{Fl,TG}(t, \lambda)$, and long-lived luminescence, $I_{Lu,TG}(t, \lambda)$, from one another.

Disentangling dual emission from a DNA-AgNC. To demonstrate the applicability of TG-FTS, we first examine a DNA-stabilized silver nanocluster (referred to as DNA-Ag$_{16}$NC), which we have previously shown exhibits dual emission with a short- (intensity averaged decay time of 2.2 ns) and long-lived (intensity averaged decay time of 76 µs) component when dissolved in D_2O[16,17]. When measuring the steady-state emission spectrum at room temperature (RT), the two components are seemingly overlapping, while they become more spectrally distinct when frozen at 77 K. In Fig. 2, we show that we can completely disentangle the emission at 77 K upon 520 nm excitation; similar results at RT are presented in Supplementary Fig. 5, where the contribution of the long-lived component is, however, much lower.
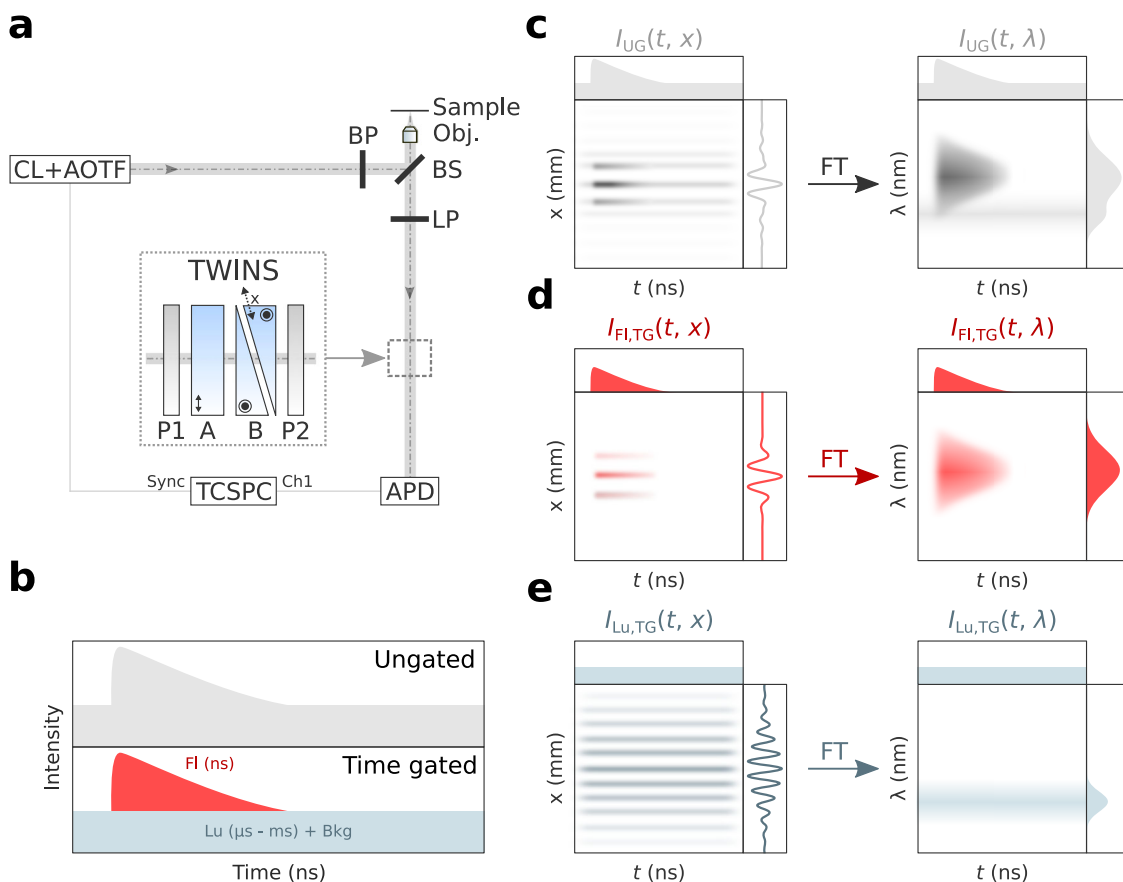
Fig. 1 Principle of TG-FTS. a Schematic of the experimental setup used to demonstrate TG-FTS on a microscope setup. **b** Illustration of time gating procedure to temporally disentangle short- (Fl, ns) and long-lived (Lu, μs-ms) contributions. **c** Illustration of how the ungated TRIM ($I_{UG}(t, x)$) and TREM ($I_{UG}(t, λ)$) of a dual-emissive species might be spectrally overlapping but temporally distinct. **d, e** Time gating $I_{UG}(t, x)$ yields TG-TRIMs, which by FT, and a series of calibrations, in turn gives disentangled TG-TREMs of the fluorescence ($I_{Fl,TG}(t, λ)$) and luminescence ($I_{Lu,TG}(t, λ)$). Abbreviations used in **a** CL supercontinuum laser, AOTF acousto-optic tunable filter, BP band pass filter, BS beam splitter, LP long pass filter, Obj. objective, APD avalanche photodiode.

The ungated TRIM and TG-TRIMs of DNA-Ag$_{16}$NC (Fig. 2a) are similar to the theoretical example in Fig. 1c–e. The ungated TRIM of DNA-Ag$_{16}$NC ($I_{UG}(t, x)$) shows a short fluorescence decay on top of a significant background. This can be seen from the map itself and the decay on top (shown on a log scale), which is obtained by integrating along the displacement axis, x. The TG-TRIMs were constructed from $I_{UG}(t, x)$, using a time gate that encompasses the entire fluorescence decay (31–50 ns). The resulting second map ($I_{Fl,TG}(t, x)$) represents the short-lived fluorescence contribution, which has been corrected for residual long-lived emission in the time gate ($-<I>$, see Supplementary Note 2 for a more detailed description of the correction procedure). The third map ($I_{Lu,TG}(t, x)$), on the other hand, only contains long-lived luminescence, as it is constructed from the photons that are detected outside the defined time gate. As there is no interferometric/spectral difference between luminescence photons detected at different times (e.g., at 15 ns or 60 ns), it is possible to represent the luminescence contribution within the fluorescence time gate as the mean of the luminescence photons outside that time gate ($<I>$, in Fig. 2). That the short- and long-lived components exhibit different frequencies in $I_{UG}(t, x)$, can more clearly be seen from the overlaid integrated interferograms $I_{Fl,TG}(x)$ and $I_{Lu,TG}(x)$ in Fig. 2b, which also shows that the short-lived component has a greater amplitude.

From each of the TRIMs, it is possible to calculate corresponding TREMs by FT (Fig. 2c); a series of calibrations are performed to ensure that the wavelength and intensity values of the TREMs are accurate (see Supplementary Note 3). The

results are similar to the schematic in Fig. 1c–e, and the TREM of DNA-Ag$_{16}$NC ($I_{UG}(t, λ)$) reveals a short- and long-lived component centered at 677 nm and 825 nm, respectively. The TG-TREMs disentangle the spectra of the short- ($I_{Fl,TG}(t, λ)$) from the long-lived ($I_{Lu,TG}(t, λ)$) states. The disentanglement of the two from the ungated spectrum is best appreciated by overlaying them (Fig. 2d).

Retrieving quantum dot emission in autofluorescent serum. Biological matrices are notorious for containing endogenous molecules that display autofluorescence, which can bury the luminescence of interest in an undesired background[18]. Two popular ways of separating autofluorescence from the signal of interested is either by using probes with anti-Stokes emission (e.g., upconversion nanoparticles[19]) or by time gating[20]. For time gating purposes, a probe with a fairly long luminescence decay is required, since the decay time of autofluorescence is usually a few nanoseconds[21]. Any emitter with an excited state lifetime that is a factor of ten or more larger than the autofluorescence, can easily be disentangled. To this end, we use semiconductor quantum dots (QDs)[22] and demonstrate how to retrieve the emission spectrum of CdTe-QDs from the dominating autofluorescence of fetal bovine serum (FBS) by TG-FTS.

The CdTe-QDs (dissolved in MQ water) and FBS yield Stokes-shifted emission with decay times of 41 ns and 5 ns, respectively, when excited at 450 nm (Supplementary Fig. 6, 7). Upon examining the decays of the unmixed constituents, a time gate is defined that encompasses the autofluorescence of FBS (Fig. 3b); emission
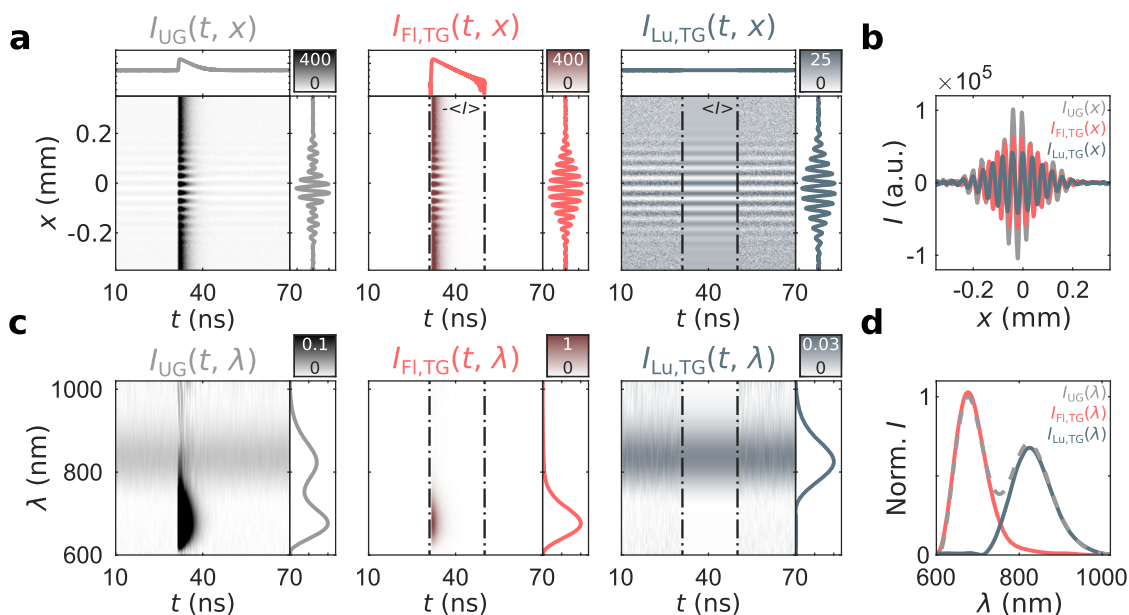
Fig. 2 TG-FTS disentangles short- and long-lived dual emission from DNA-Ag$_{16}$NC in D$_2$O at 77 K. a Ungated ($I_{UG}(t, x)$), fluorescence-gated ($I_{Fl,TG}(t, x)$), and luminescence-gated ($I_{Lu,TG}(t, x)$) TRIMs. **b** Overlay of the integrated TRIMs. **c** Ungated ($I_{UG}(t, \lambda)$), fluorescence-gated ($I_{Fl,TG}(t, \lambda)$), and luminescence-gated ($I_{Lu,TG}(t, \lambda)$) TREMs normalized to the maximum of $I_{UG}(t, \lambda)$. Note that different limits are used for each of the TREMs to highlight the different contributions. **d** Resulting spectra of the interferograms in **b**.

collected outside this time gate is accordingly entirely from the CdTe-QDs. Preparing a solution of CdTe-QDs in FBS (125 µg L^{-1}, 87.5% FBS and 12.5 % QD in MQ water, Fig. 3a) yields a luminescence decay dominated by FBS within the time gate, with some contribution of the long-lived tail from the CdTe-QDs (Fig. 3b). The TRIM of the CdTe-QD + FBS mixture shows modulation within and outside the time gate (Fig. 3c); this is even more clearly seen from the integrated interferograms overlaid in Fig. 3d. The resulting TREM shows a broad short-lived feature (FBS contribution) and a long-lived band at around 605 nm (CdTe-QD contribution, Fig. 3e). The resulting ungated spectrum is dominated by the FBS emission, and even though it only amounts to small fraction of the overall signal, the spectrum constructed from the region outside the time gate clearly reveals the Gaussian-shaped QD band at 605 nm (Fig. 3f). To confirm that we can quantitatively extract the QD emission in such a high autofluorescence background, we measured a dilution series and find that the emission intensity exhibits a linear response and that the emission maximum and full width at half max display negligible spectral deviations at the different concentrations (Supplementary Fig. 8).

Note that for emitters with luminescence decay times on vastly different time scales (e.g., for ligand-lanthanide pairs with nano- and millisecond decay times, respectively), it is straightforward to correct the amplitude of the luminescence contribution for luminescence falling within the fluorescence time gate (Supplementary Note 2). However, in the case of CdTe-QD and FBS with decay times that are relatively close (41 ns and 5 ns, respectively), it becomes more cumbersome to correct for, since the long-lived emission no longer appear as a flat background. For the data presented in Fig. 3 we opted to omit this amplitude-correction, but in Supplementary Note 4 we propose a procedure to correct the QD contribution for a better estimate of its actual amplitude. Note that knowledge about the individual decay components and the assumption that the decays are unaltered in the mixture is only required in case an amplitude correction is desired.

**Discriminating phosphorescence from the fluorescence of an organic dye.** Organic dyes with a high yield of intersystem

crossing are often used as photosensitizers in photodynamic therapy, as they are able to generate singlet oxygen or other reactive oxygen species[23]. A prerequisite for the ability of the dyes to generate singlet oxygen is that the energy difference of the triplet to ground state is sufficient to reach the first or second singlet state of molecular oxygen (around 1275 nm and 765 nm)[24]. This energy difference of the triplet state to ground state can be experimentally assessed by measuring the phosphorescence of the photosensitizer. Because phosphorescence is often outcompeted by non-radiative processes at RT, it is commonly measured at 77 K. Here we demonstrate how TG-FTS can aid in determining the triplet to ground state energy for an organic dye (rose bengal) known for its ability to create high yields of singlet oxygen[25,26].

Rose bengal (RB, Fig. 4a) belongs to the class of xanthene dyes derived from fluorescein, but with the addition of heavy atoms (i.e., iodines) for an increased triplet formation yield[27]. Exciting an aqueous solution of RB at RT at 520 nm results in a dominating short instrument response function (IRF)-limited fluorescence response (Supplementary Fig. 10). From the recorded TRIM, a time gate capturing the entire fluorescence signal is defined (31–38 ns), and TG-TREMs are prepared accordingly (Supplementary Fig. 10). While two orders of magnitude lower in intensity, we are still able to detect a low intensity long-lived phosphorescence signal (Supplementary Fig. 10c, d). Given the low phosphorescence count rate at RT, we decided to measure the emission of RB at 77 K (Supplementary Fig. 11). From the overlaid TG-TREMs (Fig. 4b), it can be seen that the fluorescence response remains IRF-limited and that the phosphorescence contribution increased significantly with an emission maximum at 737 nm (Fig. 4c). We note that the fluorescence spectrum red shifted upon freezing, which we attribute to concentration effects due to water freezing heterogeneously and the fact that we observe similar red shifts at room temperature for increasingly concentrated solutions of RB (Supplementary Fig. 12). Nonetheless, the results with TG-FTS are in line with previous findings and show that it is possible to disentangle the phosphorescence signal from the fluorescence[28].
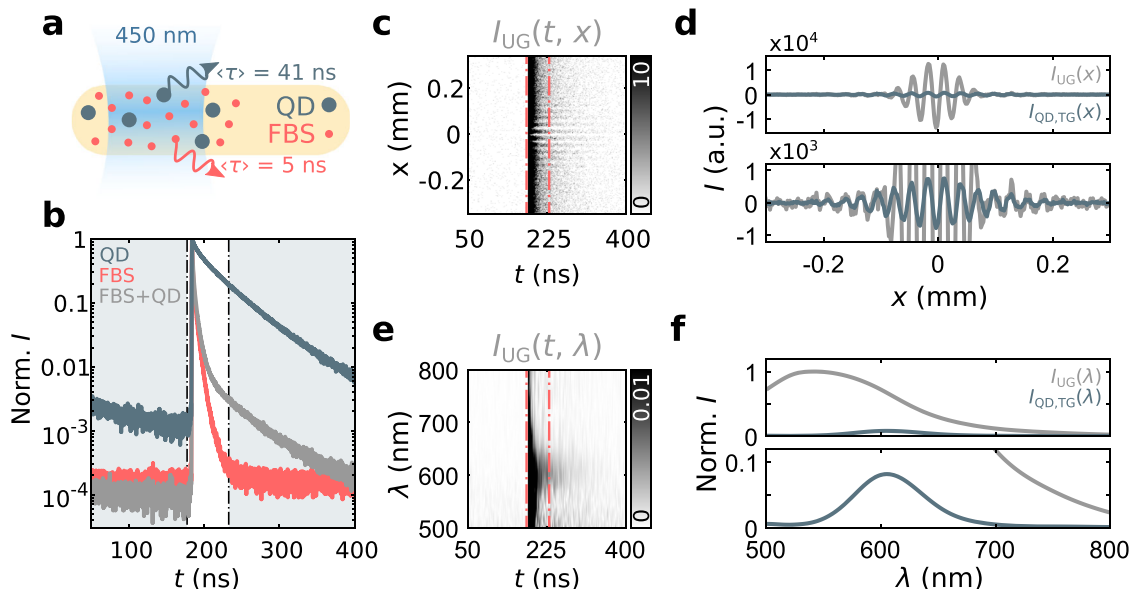
Fig. 3 TG-FTS disentangles CdTe-QD emission from FBS autofluorescence. a Cartoon illustrating the experiment where CdTe-QDs and FBS are both excited at 450 nm and emit with intensity averaged decay times of 41 ns and 5 ns, respectively. **b** Normalized luminescence decays of CdTe-QD (dissolved in MQ water), FBS, and a solution of CdTe-QD in FBS. A time gate for the CdTe-QDs is defined outside 180–230 ns (colored area). **c** UG-TRIM of the FBS+ CdTe-QD mixture with the time gate shown in red. **d** Resulting ungated ($I_{UG}(x)$) and CdTe-QD time gated ($I_{QD,TG}(x)$) interferograms with a full (top) and zoomed-in (bottom) view. **e** UG-TREM of FBS+CdTe-QD mixture. **f** Resulting spectra of the interferograms in **d** with a full (top) and zoomed-in (bottom) view.
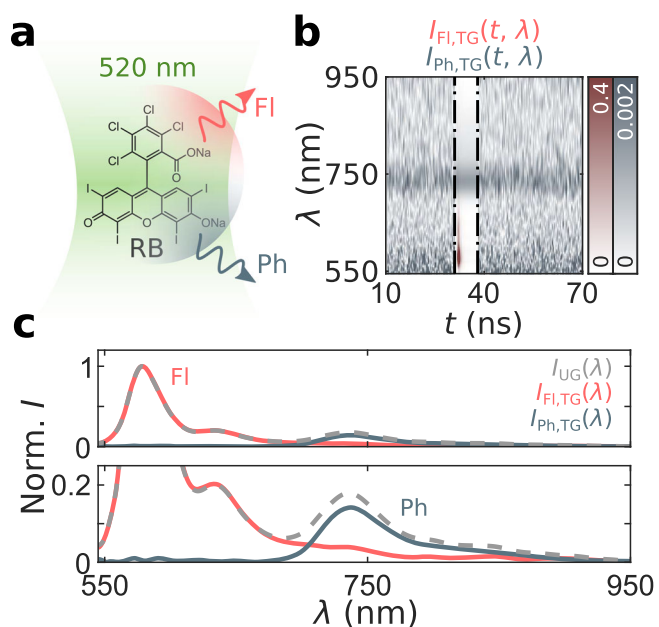
Fig. 4 TG-FTS disentangles phosphorescence and fluorescence from RB at 77 K. a Experimental configuration, where a frozen (77 K) aqueous solution of RB is excited at 520 nm, which emits short- and long-lived fluorescence and phosphorescence, respectively. **b** Overlaid TG-TREMs showing the short-lived fluorescence ($I_{Fl,TG}(t, \lambda)$, time gate from 31 to 38 ns) in red and long-lived phosphorescence ($I_{Ph,TG}(t, \lambda)$, time gate outside 31–38 ns) in blue. **c** Time gated spectra of RB showing a fluorescence peak at 579 nm (top) and a phosphorescence band at 737 nm (bottom).

Separating lanthanide from ligand emission. Lanthanide-based emitters have found applications in many areas, partly due to their key features which include narrow emission lines and long-lived excited state lifetimes in the micro- to milliseconds range[29]. While long lifetimes are beneficial for time gated signal collection

or imaging, they also imply small transition probabilities which makes direct excitation challenging. This issue is often bypassed by using an antenna (made out of an organic chromophore) with a high excitation cross-section that can sensitize the lanthanide luminescence[30]. Unless complete energy transfer is achieved, the antenna fluorescence can cover the lanthanide luminescence. Here we show for a commonly used lanthanide complex (Lumi4-Tb)[31,32], how TG-FTS can be used to untangle the contributions from both ligand and lanthanide.

Upon excitation in the UV, the ligand sensitizes the emission of Tb^{3+}, which emits on the millisecond timescale[33]. Due to incomplete sensitization, residual fluorescence from the ligand is also observed on the nanosecond timescale (Fig. 5a). A time gate encompassing the ligand fluorescence (65–90 ns) is defined from the measured TRIM (Supplementary Fig. 13) and is used for preparing TG-TREMs (Fig. 5b). From the overlaid TG-TREMs, the tailing short-lived fluorescence from the ligand can be observed alongside the narrow emission bands of Tb^{3+}, which are constant in the entire detection window. The resulting spectra (Fig. 5c) of the integrated interferograms (Supplementary Fig. 13d) clearly reveal the characteristic emission bands of Tb^{3+} ($I_{Tb3+,TG}(\lambda)$), which are otherwise entangled with the contribution of the ligand emission ($I_{Ligand,TG}(\lambda)$) when measured ungated ($I_{UG}(\lambda)$). With TG-FTS, we can disentangle the Tb^{3+} luminescence from the ligand fluorescence and unambiguously assign the transitions of Tb^{3+} to $^5D_4 \rightarrow {}^7F_J$ (for $J = 3$–6)[34].

Measuring emission spectra without optical filters under ambient light. As a final demonstration of TG-FTS, we measure the emission spectrum of indocyanine green (ICG) under ambient room light (from fluorescent light bulbs) without excitation or emission filters (Fig. 6a); a situation that might prove valuable for fluorescence guided surgery purposes[35,36]. This poses as a very challenging setting with many overlapping signals, which is even further complicated by the IRF-limited decay of ICG (Supplementary Fig. 14). Nonetheless, TG-FTS allows for disentangling all three contributions, as will be demonstrated here.

From the recorded TRIM, a time gate encompassing the room light, which appears as a long-lived signal, is defined (TG$_{RL}$, Fig. 6b). In the microscope setting we used, focusing into the
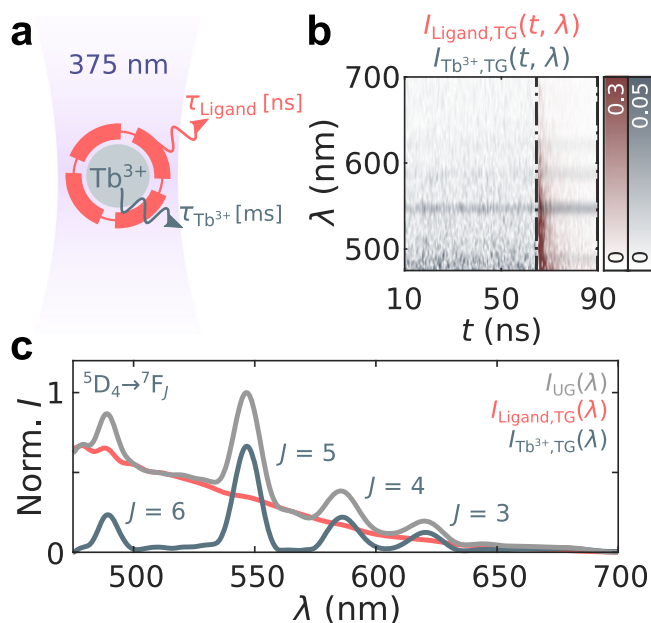
Fig. 5 TG-FTS disentangles lanthanide from ligand emission. a Cartoon of the experiment, where UV light excites the ligand, which fluoresces on the nanosecond timescale and sensitizes the Tb^{3+}, which emits on the milisecond timescale. **b** Overlaid TG-TREMs showing the fluorescence of the ligand ($I_{Ligand,TG}(t, \lambda)$, time gate from 65 to 90 ns) in red and luminescence of Tb^{3+} ($I_{Tb3+,TG}(t, \lambda)$, time gate from 10 to 65 ns) in blue. **c** Spectra of the ungated ($I_{UG}(\lambda)$), ligand gated ($I_{Ligand,TG}(\lambda)$), and Tb^{3+} gated ($I_{Tb3+,TG}(\lambda)$) integrated interferograms. The $^5D_4 \rightarrow {}^7F_J$ transitions of Tb^{3+} for $J = 3$–6 have been assigned based on previous reports[34].

solution led to the detection of scattered excitation light before the onset of ICG emission. Hence, it is possible to define two time gates; one which has scattered excitation light (TG$_{Ex}$) and another with a combination of scattered excitation light and ICG emission (TG$_{Ex+ICG}$, Fig. 6c). The ungated integrated interferogram and the corresponding spectrum (Fig. 6d) reveals a complex structure with many spectral features. By only considering photons falling within TG$_{RL}$, it is possible to construct an interferogram of the room light and by FT obtain the resulting spectrum (Fig. 6e), which shows relatively sharp lines in the visible range, characteristic of fluorescent light bulbs containing rare earth phosphors. Removing the room light contribution from the ungated interferogram yields an interferogram which has contributions from the excitation light and ICG ($I_{Ex+ICG}(x)$, Supplementary Figs. 15, 16).

Since there is no ICG signal within TG$_{Ex}$, it is possible to use photons within this time gate to obtain an interferogram and spectrum of the excitation light, which shows a single peak at 790 nm (Fig. 6f). We note that a similar approach was recently presented by Ksantini et al. to improve the signal to noise ratio of the Raman signal with respect to the fluorescence background by time gating the signal of interest close to the IRF limited response of a pulsed laser[37]. By subtracting a scaled amount of $I_{Ex}(x)$ from $I_{Ex+ICG}(x)$, it is possible to retrieve the interferogram and emission spectrum of ICG revealing an emission maximum at 808 nm and a vibronic shoulder around 900 nm (Fig. 6g, see Supplementary Note 5 for details on disentanglement procedure). In case there is no laser specific signal that is temporally separated from the fluorescence response (i.e., if the ICG signal is present in the entire excitation window), it would be possible to deliberately introduce a part of the excitation light in the detection path, bypassing the sample. This could ensure a region in the TAC window with excitation light only to be used for TG$_{Ex}$. Alternatively, it is also possible to first record an interferogram from the laser alone and subtract a scaled amount of $I_{Ex}(x)$ from $I_{Ex+ICG}(x)$ to retrieve $I_{ICG}(x)$. A final option to retrieve $I_{ICG}(x)$
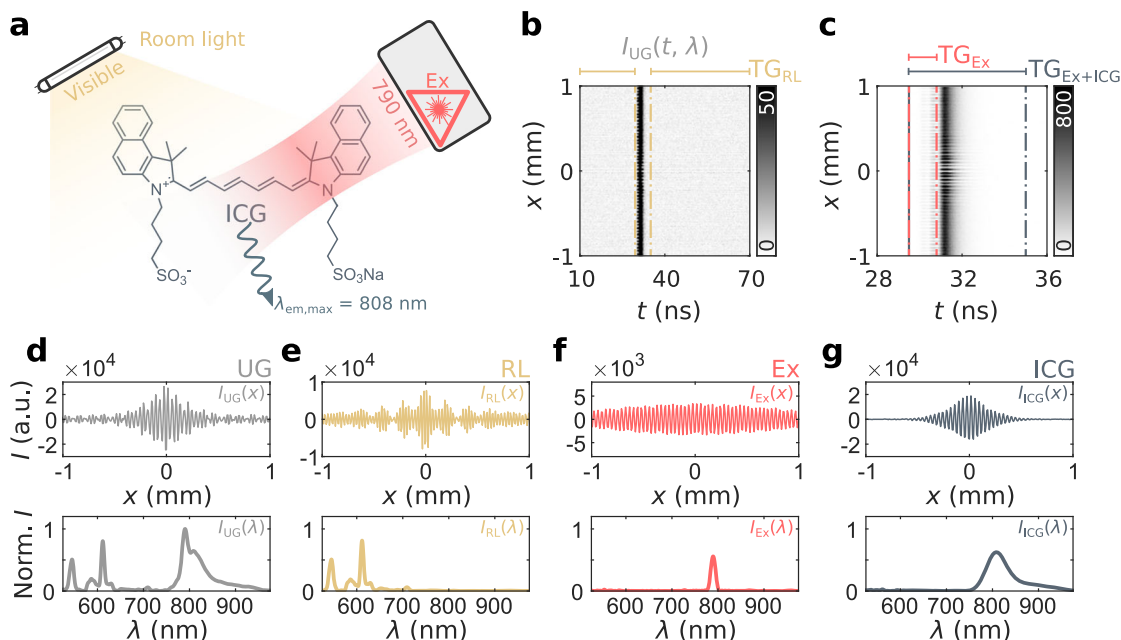
Fig. 6 TG-FTS can disentangle the emission spectrum of ICG from excitation light and room light without excitation or emission filters. a Cartoon illustrating the experiment, where ICG is excited at 790 nm under room light illumination. **b** TRIM with the room light time gate (TG$_{RL}$) shown. **c** Zoom-in of the same TRIM to highlight the time gates used for excitation light (TG$_{Ex}$) and the combined excitation and ICG signal (TG$_{Ex+ICG}$). **d** Ungated integrated interferogram and the corresponding normalized spectrum. **e, f, g** Disentangled interferograms and the corresponding spectra (normalized to $I_{UG}(\lambda)$) of room light (RL), excitation light (Ex), and ICG, respectively.

from $I_{\text{Ex+ICG}}(x)$, would be to use the fact that the interferogram of a spectrally narrow excitation source is expected to have a single sinusoidal frequency feature, which could be fitted and subtracted.

Conclusions

In summary, we have demonstrated TG-FTS, a technique for simultaneously measuring and disentangling overlapping spectral features of short- (ns) and long-lived (µs–ms) luminescence signals. The technique is based on combining interferometry with TCSPC, which provide spectral and temporal information, respectively. In TG-FTS, spectral disentanglement is ensured by temporally gating photons that originate from short- or long-lived states or species. We demonstrated the applicability of TG-FTS for some of the most commonly used luminophore classes, including organic dyes, semiconductor QDs, lanthanide complexes, and metal nanoclusters. TG-FTS, for instance, proved capable of retrieving the spectral features of a QD from the dominating FBS autofluorescence, discriminating lanthanide emission from that of the ligand, and retrieving the NIR emission spectrum of an organic dye in an experimental setting complicated by the presence of ambient room light and scatter from the excitation source as a result of using neither excitation nor emission filters.

Our current implementation of TG-FTS can resolve the decay time of short-lived (ns) species, but it is currently unable to capture the decay time of long-lived species (µs–ms). We recently demonstrated how a burst mode approach could be useful for simultaneously determining short- and long-lived decay times and we hope to implement this in the near future for TG-FTS[16]. While the examples presented here were implementations of TG-FTS on a microscope setup, it could equally well be implemented in a cuvette based configuration[14,15,38]. Additionally, while we demonstrated an emission-based implementation of TG-FTS, it is equally applicable for measuring time gated excitation spectra[15].

Methods

Materials. COOH functionalized CdTe quantum dots, rose bengal, indocyanine green, $AgNO_3$, ammonium acetate, and $NaBH_4$ were acquired from Sigma Aldrich. Lumi4-Tb conjugated to streptavidin was purchased from PerkinElmer. DNA was purchased from Integrated DNA Technologies and D_2O was purchased from Eurisotop. FBS was purchased from ThermoFisher. All chemicals were used as received without further purification.

TG-FTS experimental setup. All TG-FTS measurements were performed on a home-built microscope setup. A fiber coupled (FD7-PM, NKT Photonics) continuum white-light laser (SuperK EXTREME EXB-6, NKT Photonics) was used as an excitation source delivering wavelengths in the range of 415–1100 nm by sending the continuum output through an acousto-optic tunable filter (SuperK SELECT, NKT Photonics). The excitation light was in most cases cleaned up by a band-pass filter before being expanded (BE05M-A, Thorlabs). The excitation light was then reflected by a 30:70 beam splitter (XF122, Omega Optical) and sent through an objective (see below), which focused the laser onto the sample. Luminescence was collected from the same objective, and residual excitation light was usually removed with a long pass filter. The emission light was directed through the TWINS device (GEMINI, NIREOS) and finally detected on an avalanche photodiode (SPCM-AQRH-14-TR, Excelitas Technologies) connected to a single photon counting module (SPC-830, Becker & Hickl). Count rates were adjusted to be significantly lower than the repetition rate in order to avoid pile-up effects. The time axis in the TRIMs and TREMs is used as it is obtained from the experiment, though it could be arbitrarily shifted to have the fluorescence decay start at $t = 0$ ns. Official LabVIEW routines from NIREOS and Becker & Hickl were modified and combined to allow for measuring TRIMs.

Note that an oil immersion objective was used (UPlanSAPO 100× NA = 1.3, Olympus) for experiments conducted at room temperature, and an air objective (CPlanFLN 10×, NA = 0.3, Olympus) was used for low temperature (77 K) experiments. A temperature-controlled stage (LTS 350 and LNP, Linkam) was used to ensure cryogenic temperatures. Furthermore, for experiments with the Lumi4-Tb sample, a 375 nm excitation laser diode (LDH-P-C-375, PicoQuant) was instead used in addition to a change of the beam splitter with a 442 nm dichroic mirror (Di02-R442, Semrock). Details about excitation wavelength, repetition rate,

excitation and emission filters, and interferometer scans settings used for each presented experiment can be found in Supplementary Note 7.

TG-FTS data analysis. The measured TRIMs were subsequently analyzed in MATLAB with home-written routines for the preparation of TREMs and TG-TRIMs/TG-TREMs. A detailed description of the workflow for preparing TREMs from recorded TRIMs can be found in Supplementary Note 1. Meanwhile, Supplementary Note 2 describes the procedure of time gating data in detail.

DNA-Ag$_{16}$NC synthesis. DNA–Ag$_{16}$NC was synthesized according to the protocol described in Cerretani et al.[17], and is described in detail in Supplementary Note 6.

Data availability
The data that support the findings of this work are available at https://doi.org/10.17894/ucph.bac6f468-c961-4e62-8bcb-d4a15212e2f5.

Code availability
The code used in this paper is available at https://doi.org/10.17894/ucph.bac6f468-c961-4e62-8bcb-d4a15212e2f5.

References

1. Hong, G. et al. Through-skull fluorescence imaging of the brain in a new near-infrared window. *Nat. Photonics* **8**, 723–730 (2014).
2. Kacenauskaite, L. et al. Rational design of bright long fluorescence lifetime dyad fluorophores for single molecule imaging and detection. *J. Am. Chem. Soc.* **143**, 1377–1385 (2021).
3. Yasuda, M. & Akimoto, T. High-contrast fluorescence imaging based on the polarization dependence of the fluorescence enhancement using an optical interference mirror slide. *Anal. Sci.* **31**, 139–143 (2015).
4. Marriott, G. et al. Optical lock-in detection imaging microscopy for contrast-enhanced imaging in living cells. *Proc. Natl Acad. Sci. USA* **105**, 17789–17794 (2008).
5. Liisberg, M. B., Lahtinen, S., Sloth, A. B., Soukka, T. & Vosch, T. Frequency encoding of upconversion nanoparticle emission for multiplexed imaging of spectrally and spatially overlapping lanthanide ions. *J. Am. Chem. Soc.* **143**, 19399–19405 (2021).
6. Evans, D. et al. Determination of the optical band-gap energy of cubic and hexagonal boron nitride using luminescence excitation spectroscopy. *J. Phys.: Condensed Matter* **20**, 075233 (2008).
7. Roura, P., López-de Miguel, M., Cornet, A. & Morante, J. Determination of the direct band-gap energy of InAlAs matched to InP by photoluminescence excitation spectroscopy. *J. Appl. Phys.* **81**, 6916–6920 (1997).
8. Campillo, A. & Shapiro, S. Picosecond streak camera fluorometry-a review. *IEEE J. Quantum Electron.* **19**, 585–603 (1983).
9. Méhes, G., Nomura, H., Zhang, Q., Nakagawa, T. & Adachi, C. Enhanced electroluminescence efficiency in a spiro-acridine derivative through thermally activated delayed fluorescence. *Angew. Chem. Int. Ed.* **51**, 11311–11315 (2012).
10. Komura, M. & Itoh, S. Fluorescence measurement by a streak camera in a single-photon-counting mode. *Photosynth. Res.* **101**, 119–133 (2009).
11. Cerretani, C., Carro-Temboury, M. R., Krause, S., Bogh, S. A. & Vosch, T. Temperature dependent excited state relaxation of a red emitting DNA-templated silver nanocluster. *Chem. Commun.* **53**, 12556–12559 (2017).
12. Becker, W. *Advanced time-correlated single photon counting applications*. Vol. 111 (Springer, 2015).
13. Perri, A. Visible and near-infrared Fourier transform spectroscopy with a common-path interferometer. *J. Phys. B: At. Mol. Opt. Phys.* **54**, 113001 (2021).
14. Perri, A. et al. Time-and frequency-resolved fluorescence with a single TCSPC detector via a Fourier-transform approach. *Opt. Express* **26**, 2270–2279 (2018).
15. Perri, A. et al. Excitation-emission Fourier-transform spectroscopy based on a birefringent interferometer. *Opt. Express* **25**, A483–A490 (2017).
16. Liisberg, M. B., Krause, S., Cerretani, C. & Vosch, T. Probing emission of a DNA-stabilized silver nanocluster from the sub-nanosecond to millisecond timescale in a single measurement. *Chem. Sci.* **13**, 5582–5587 (2022).
17. Cerretani, C., Palm-Henriksen, G., Liisberg, M. B. & Vosch, T. The effect of deuterium on the photophysical properties of DNA-stabilized silver nanoclusters. *Chem. Sci.* **12**, 16100–16105 (2021).

18. Hong, G., Antaris, A. L. & Dai, H. Near-infrared fluorophores for biomedical imaging. *Nat. Biomed. Eng.* **1**, 1–22 (2017).

19. Lahtinen, S. et al. Thulium-and erbium-doped nanoparticles with poly (acrylic acid) coating for upconversion cross-correlation spectroscopy-based sandwich immunoassays in plasma. *ACS Appl. Nano Mater.* **4**, 432–440 (2020).

20. Fleischer, B. C., Petty, J. T., Hsiang, J.-C. & Dickson, R. M. Optically activated delayed fluorescence. *J. Phys. Chem. Lett.* **8**, 3536–3543 (2017).

21. Zhang, K. Y. et al. Long-lived emissive probes for time-resolved photoluminescence bioimaging and biosensing. *Chem. Rev.* **118**, 1770–1839 (2018).

22. Algar, W. R. et al. Quantum dots as simultaneous acceptors and donors in time-gated forster resonance energy transfer relays: characterization and biosensing. *J. Am. Chem. Soc.* **134**, 1876–1891 (2012).

23. Ormond, A. B. & Freeman, H. S. Dye sensitizers for photodynamic therapy. *Materials* **6**, 817–840 (2013).

24. Bregnhøj, M., Blazquez-Castro, A., Westberg, M., Breitenbach, T. & Ogilby, P. R. Direct 765 nm optical excitation of molecular oxygen in solution and in single mammalian cells. *J. Phys. Chem. B* **119**, 5422–5429 (2015).

25. Neckers, D. Rose bengal. *J. Photochem. Photobiol. A: Chem.* **47**, 1–29 (1989).

26. Redmond, R. W. & Gamlin, J. N. A compilation of singlet oxygen yields from biologically relevant molecules. *Photochem. Photobiol.* **70**, 391–475 (1999).

27. Fleming, G., Knight, A., Morris, J., Morrison, R. & Robinson, G. Picosecond fluorescence studies of xanthene dyes. *J. Am. Chem. Soc.* **99**, 4306–4311 (1977).

28. Ludvíková, L. et al. Photochemistry of rose bengal in water and acetonitrile: a comprehensive kinetic analysis. *Phys. Chem. Chem. Phys.* **18**, 16266–16273 (2016).

29. Bünzli, J. C. G. & Piguet, C. Taking advantage of luminescent lanthanide ions. *Chem. Soc. Rev.* **34**, 1048–1077 (2005).

30. Latva, M. et al. Correlation between the lowest triplet state energy level of the ligand and lanthanide (III) luminescence quantum yield. *J. Lumin.* **75**, 149–169 (1997).

31. Morgner, F. et al. A quantum-dot-based molecular ruler for multiplexed optical analysis. *Angew. Chem. Int. Ed.* **49**, 7570–7574 (2010).

32. Tsai, H.-Y. & Algar, W. R. A dendrimer-based time-gated concentric FRET configuration for multiplexed sensing. *ACS nano* **16**, 8150–8160 (2022).

33. Chen, T. et al. Time gated luminescence imaging of immunolabeled human tissues. *Anal. Chem.* **89**, 12713–12719 (2017).

34. Carnall, W., Fields, P. & Rajnak, K. Electronic energy levels of the trivalent lanthanide aquo ions. III. Tb3+. *J. Chem. Phys.* **49**, 4447–4449 (1968).

35. Vahrmeijer, A. L., Hutteman, M., Van Der Vorst, J. R., Van De Velde, C. J. & Frangioni, J. V. Image-guided cancer surgery using near-infrared fluorescence. *Nat. Rev. Clin. Oncol.* **10**, 507–518 (2013).

36. Cosco, E. D., Lim, I. & Sletten, E. M. Photophysical properties of indocyanine green in the shortwave infrared region. *ChemPhotoChem.* **5**, 727–734 (2021).

37. Ksantini, N. et al. Time-gated interferometric detection increases Raman scattering to fluorescence signal ratio in biological samples. *J. Biophotonics* **15**, e202100188 (2022).

38. Ghosh, S. et al. Broadband optical activity spectroscopy with interferometric Fourier-transform balanced detection. *ACS Photonics* **8**, 2234–2242 (2021).

Author contributions

M.B.L. and T.V. conceived the idea. M.B.L. conducted the experiments and analyzed the data. M.B.L. and T.V. wrote the paper.

Competing interests

The authors declare no competing interests.

Additional information

Supplementary information The online version contains supplementary material available at https://doi.org/10.1038/s43246-023-00386-z.

Correspondence and requests for materials should be addressed to Mikkel Baldtzer Liisberg or Tom Vosch.

Peer review information *Communications Materials* thanks the anonymous reviewers for their contribution to the peer review of this work. Primary Handling Editor: Jet-Sing Lee.

Reprints and permission information is available at http://www.nature.com/reprints

Publisher's note Springer Nature remains neutral with regard to jurisdictional claims in published maps and institutional affiliations.